submitted to *BSSA*

Impact of aseismic transients on seismicity parameter estimations

Sebastian Hainzl[1], Olga Zakharova[1], David Marsan[2]

[1] *GFZ German Research Centre for Geosciences, Potsdam, Germany*

[2] *ISTerre, CNRS, Universite de Savoie, Le Bourget du Lac, France*

31 July 2012

ABSTRACT

The epidemic-type aftershock sequence (ETAS) model has been shown to describe successfully the spatiotemporal evolution of the statistical seismicity properties, if earthquake triggering is related to tectonic forcing and earthquake-induced stress changes. However, seismicity is locally often dominated by stress changes related to transient aseismic processes. To avoid erroneous model fitting leading to biased forecasts, it is important to account for those transients. We apply a recently developed iterative algorithm based on the ETAS model to identify the time-dependent background and ETAS-parameters simultaneously. We find that this procedure works well for synthetic data sets if catalog errors are appropriately considered. Vice versa, ignoring the time-dependence leads to significantly biased parameter estimations. In particular, the α-value describing the magnitude-dependence of the triggering kernel can be strongly underestimated if transients are ignored. Low α-values have been previously found for swarm activity, for which transient aseismic processes are expected to play a major role. These observed anomalously low α-values might thus indicate the importance of transient forcing, rather than being due to differences in the earthquake-earthquake trigger mechanism. To explore this, we apply the procedure systematically to earthquake clusters detected in southern California and to earthquake swarm activity in Vogtland/Western Bohemia. While low α-

values are mostly shown to be a consequence of catalog errors and time-dependent forcing but not related to different earthquake-earthquake interaction mechanisms, some significant low values are observed in high heat flow areas in California, confirming the existence of thermal control on earthquake triggering.

1 INTRODUCTION

Interactions between earthquakes have been long recognized to be an important mechanism for earthquake triggering. A large fraction of earthquakes in instrumental catalogs are aftershocks (Reasenberg 1985)), which can be explained by stress changes of previous events (Dieterich 1994; Harris 1998; Stein 1999). Vice versa, earthquakes which cannot be attributed to any preceding earthquake are likely to be related to aseismic sources. Usually those events are associated to the stationary aseismic process of stress build-up due to constant tectonic plate motions. While this might be correct on long-time scales, transient aseismic forcing such as magma intrusion (Toda et al. 2002), fluid flow (Miller et al. 2004) or slow slip events (Holtkamp and Brudzinski 2011) are frequently occurring on short-time scales. Because these aseismic processes are usually not directly observable, aseismic transients are generally ignored in seismicity modeling and forecasting. However, modeling of transient aseismic triggering is important not only because it can help to retrieve important information about the underlying mechanism, but also because the estimation of seismicity parameters can be - as we will show - strongly biased if the transients are ignored. This can directly affect our ability for short-time forecasting or seismic hazard assessment because both rely on a proper knowledge of the earthquake-earthquake interactions to model the clustering properties or decluster the seismicity, respectively.

An important seismicity parameter is the α-parameter, which determines how the number of aftershocks depends on the mainshock magnitude m. While there is good empirical evidence that the aftershock productivity grows exponentially with m as $\sim e^{\alpha m}$, the exact value of α varies substantially between empirical studies, in particular, between windows-based cluster definitions and epidemic type aftershock sequence (ETAS) model fits. The former class yields typically values around $\ln(10)$ (Helmstetter et al. 2005), although Christophersen and Smith (2008) showed

that the inferred α-value is up to the specific choice of dependence of the spatial windows on the mainshock magnitude. An $\alpha = \ln(10)$ value gives a 10^m-scaling, which can be expected for static stress triggering (Hainzl et al. 2010). Furthermore, α would be close to the value of the exponent of the Gutenberg-Richter law, $N(m) \propto 10^{-bm} = e^{\ln(10)bm}$, i.e $\alpha \approx \ln(10)b$. This would imply self-similarity of the triggering process, in particular, the cumulative effect of earthquakes in different magnitude bins would be the same. However, those results are based on comparing the total aftershock productivity of many mainshocks with different magnitudes. More sophisticated models, which differentiate between direct and secondary aftershock activity, can estimate the α-parameter for individual sequences and often find significantly smaller α-values (Ogata 1992; Marsan and Lengliné 2008). Hainzl et al. (2008) showed that an underestimation of α can result in the latter case from assuming spatial isotropy of aftershock occurrence, which in fact aligns along the mainshock rupture. They also demonstrated the severe effect of such a parameter-bias on forecasts of ongoing aftershock sequences. However, the anisotropic aftershock distributions cannot explain small α-estimations, which are based only on time and magnitude information without using the hypocenter information. In particular, very small values, $\alpha < 1$, are found for swarm activity, e.g. in Japan and Central Europe, and water-injection induced seismicity (Ogata 1992; Hainzl and Ogata 2005; Lombardi et al. 2006; Lei et al. 2008). These results could have important consequences for triggering mechanisms, because the cumulative effect of smaller events in earthquake swarms would then dominate compared to that of larger earthquakes. It is important to stress that low α-values, if they are real, preclude earthquake forecasting: since small shocks then dominate the triggering budget, a reliable forecast would require precise knowledge of these small sources, down to the smallest possible rupture length, a more than challenging task.

In this study, we show that small α-values inverted by means of the space-independent ETAS model do not necessarily point to differences in the earthquake-earthquake interaction mechanism; they can simply result from neglecting underlying aseismic transients. This might explain the observed small α-values in the cases of earthquake swarms or induced seismicity, where aseismic sources such as fluid flows are expected or known.

We firstly introduce in section 2 the recently developed approach by Marsan et al. (2012),

which we used for detecting time-dependent aseismic forcing. A detailed analysis of synthetic earthquake sequences is presented in Sec. 3 to illustrate the effect of ignoring transient forcing in seismicity parameter estimations. Then we apply the methodology to recent swarm activity in Western Bohemia and earthquake clusters in southern California (Sec. 4). Finally, our results are discussed and summarized in last two sections.

2 METHOD

The method for detecting time-dependent background forcing has been recently introduced by Marsan et al. (2012). The approach is based only on the time and magnitude information of the earthquake occurrence (t_i, m_i with $i = 1, \ldots N$). The rational is to separate the background forcing rate $\mu(t)$ and the contribution $\nu(t)$ related to earthquake-earthquake triggering, where the observed earthquake rate $\lambda(t)$ is assumed to be a linear superposition of both terms, $\lambda(t) = \mu(t) + \nu(t)$. The interaction term $\nu(t)$ is modeled using the epidemic type aftershock sequence (ETAS) model (Ogata, 1988)

$$\nu(t) = \sum_{i:t_i<t} K e^{\alpha(m_i - m_c)} (c + t - t_i)^{-p} \ , \tag{1}$$

where c and p are the parameters of the Omori-Utsu aftershock decay law (Utsu et al. 1995). The constants K and α describe the magnitude-dependent aftershock productivity and m_c is the lower magnitude cut of the analyzed catalog.

The algorithm for the model estimation consists of the following steps:

(0) Start with non-zero constant background rate $\mu(t) = \mu_0$

(1) Estimate the ETAS-parameters K, α, c, p by maximizing the log-likelihood (LL) value.

(2) Calculate probabilities that the events belong to background:

$$w_i = \mu(t_i)/(\mu(t_i) + \sum_{k:t_k<t_i} K e^{\alpha(m_k - m_c)} (c + t_i - t_k)^{-p})$$

(3) Estimate the time-dependent background rate using the n-nearest neighbors:

$$\mu(t_i) = \sum_{k=i-n/2}^{i+n/2} w_k/(t_{i+n/2} - t_{i-n/2})$$

(4) Repeat with step (1) until convergence of both the ETAS parameters and the background rate is reached.

To select the appropriate smoothing window n, the Akaike Information Criterion (AIC) is used: n must minimize $AIC = 2(N/n - LL(n))$. Here N/n is a proxy for the number of free parameters in $\mu(t)$, and penalizes models with small n values that allow $\mu(t)$ to vary too quickly.

3 SYNTHETIC TESTS

We firstly analyze the effect of time-dependent aseismic forcing and catalog incompleteness for synthetic simulations, where the underlying dynamics is known. For that purpose, we performed ETAS simulations with a set of typical triggering parameters $K = 0.015, \alpha = 1.84, c = 0.01$ day$^{-1}, p = 1.2$ and Gutenberg-Richter distributed magnitudes with a b-value of 1. These parameters refer to a theoretical branching parameter of about 0.8, which means that on average 80% of the earthquakes in the catalogs are aftershocks. However, this value is reached only on long-time scales, while most short catalogs consist of only small magnitude events leading to a smaller percentage of aftershocks. Anyway, the aftershock percentage exceeds typically 50%. For the background term $\mu(t)$ of the ETAS model, we test three different versions described below. In each case, we analyzed 100 random independent simulations for a statistical evaluation. A summary of all parameters and definitions of our synthetic simulations is shown in Table 1.

3.1 Effect of time-dependence

We explored the effect of two different types of time-dependent aseismic forcing on the parameter estimation. In one kind of simulations (ETAS-1), the temporal changes of the background forcing are smooth. The second type (ETAS-2) simulates the effect expected for an underlying aseismic stress step such as related to slow slip events. In this case, the aseismic transient triggering is modeled by a Omori-Utsu-type decaying rate. Two examples of ETAS-1 and ETAS-2 simulations are shown in Fig. 1. In addition to these two types, we also analyzed simulations with constant background rate (ETAS-0) for comparison.

For each of these simulations, we estimated the ETAS-parameters on the one hand with the

standard approach assuming constant background forcing and, on the other hand, with the new iterative method taking potential time-dependent forcing into account (see Sec. 2). The results for $N_b = 500$ background events are shown in Fig. 2. Along with those for smaller data sets ($N_b = 100$), our findings can be summarized in the following way:

(i) In the case of the ETAS-0 simulations with constant background forcing, both methods yield similar unbiased estimations of the true underlying parameters. In particular, the time-dependent method by Marsan et al. (2012) correctly identifies in almost all the cases the constant background rate, even in the case of small data sets (100 background events).

(ii) Vice versa, in the case of the simulations with time-dependent forcing (ETAS-1 and ETAS-2), the method by Marsan et al. (2012) find a time-dependent forcing as preferred solution in almost all cases. Thus, the new method is able to detect aseismic transients in these data sets.

(iii) The estimation of the ETAS-parameters assuming constant background forcing yields strongly biased aftershock productivity parameters if aseismic forcing is present. In particular, the parameters K and α are biased, while the Omori-Utsu parameters c and p are less affected. K is overestimated and α is significantly underestimated. As a consequence, the estimated background rate is only in the order of 20% of the true value.

(iv) In the same case, the new method yields almost unbiased estimates. In particular, the α-value is well-recovered with moderate uncertainties.

3.2 Effect of catalog errors

Besides transient forcing, catalog problems can also lead to biases in parameter estimates, in particular towards low α-values. To show this, we analyzed ETAS simulations (ETAS-0), which were artificially manipulated to represent three different types of catalog problems, namely (i) underestimated completeness; (ii) time-varying completeness; and (iii) missing events directly after earthquakes. Namely:

(i) Underestimated (time-independent) completeness implies that the data set is incomplete at low magnitudes. We simulate this by removing earthquakes according to a probability $\mathrm{erfc}((m - m_c)/\sqrt{2}\sigma_m)$ with $\sigma_m = 0.5$, where erfc is the complementary error function. This means e.g.

that a $m = m_c + 0.5$ event remains in the catalog with a probability of 0.68 and a magnitude $m = m_c+1$ event with probability of 0.95. This erfc-shape is empirically found when investigating the probability of earthquake detection in regional earthquake catalogs (e.g. Ogata and Katsura 1993; Daniel et al., 2008).

(ii) Time-dependent incompleteness: All earthquakes with $m \leq m_c+0.5$ are removed in the time window between 35 and 65 days.

(iii) Incompleteness after events: To account for the observed incompleteness of catalogs after mainshocks (Kagan 2004), we adopt the estimated incompleteness function for California, $m_{cut}(m, \Delta t) = m - 4.5 - 0.75 \log_{10}(\Delta t)$, where Δt is the time (in days) after an earthquake with magnitude m (Helmstetter et al. 2006). We removed all earthquakes from the simulated catalogs for which the magnitude m_i does not fulfill the condition $m_i \geq m_{cut}(m_j, t_i - t_j)$ related to any preceding earthquake $j < i$.

Examples for all three cases are shown in Fig. 3. For statistical evaluation, we again analyzed 100 synthetic catalogs in each case.

The estimated ETAS-parameters are summarized in Table 2. In particular, we found that removing about half of the events from the catalog in case (i) leads only to a lowering of K but not to any bias in the other parameters. Thus this case cannot be responsible for low α-values. However, the other two cases lead to a significant underestimation the α-parameter. This can be understood because in case (ii) the missing events in the time period of 30 days have a similar effect as a decrease of the background rate during this time. In case (iii), the scaling of the incompleteness time period with the mainshock magnitude lowers the apparent productivity of larger events compared to that of lower magnitudes. In the latter case, the bias of α is however quite small as long as c is not very small (e.g. a median value of $\alpha = 1.71$ instead of the true underlying value of 1.84 is estimated in our standard case of $c = 0.01$ days), but becomes significant for small c-values. We repeated the analysis for simulations with $c = 0.0007$ days (1 min) for which we rescaled the K-value to 0.008 to restore approximately the same branching parameter. In this case, the maximum likelihood method yields a value of 1.54.

This analysis shows that catalog errors of type (ii) and (iii) both lead to significant biases in the α-estimation. However, these biases can be avoided by reducing the likelihood space, i.e. by restricting the number of earthquakes and/or the time-interval for which the parameters are optimized. In particular, we investigated two restrictions of the likelihood space, while the observation space (used for the calculation of the rate function, Eq. 1) remains the same: optimization is only done for (a) larger earthquakes, $m \geq m_c + 0.5$ (applied to case ii), and (b) events outside the incompletely recorded time-periods directly after earthquakes (applied to case iii). We find that these restrictions help to avoid the bias in the parameter estimation (see Tab. 2). Thus for the applications in the following section, we applied both restrictions to the likelihood space.

4 APPLICATIONS

4.1 Western Bohemia swarms

Episodic occurrence of earthquake swarms is well-known in the region in West Bohemia/Vogtland, Central Europe, with the most intensive earthquake activity recorded in the years 1896/97, 1903, 1908/09, 1985/86, 2000, and 2008. Since 1994, the Novy Kostel area has been monitored by the local seismic network WEBNET (see http://www.ig.cas.cz/en/structure/observatories/west-bohemia-seismic-network-webnet) providing high quality data, which enable detailed studies of the triggering mechanisms and driving forces of the West Bohemia/Vogtland swarms based on seismicity data. Due to the presence of close-by CO_2 emanations and observed correlations of their isotopic content with swarm activity (Braeuer et al. 2007), episodic intrusions of fluid or magma are likely to be one of the driving forces of the observed earthquake clusters. This interpretation was confirmed by analysis of the seismicity showing a systematic temporal changes of the clustering properties and frequency-magnitude distribution during swarm activity (Hainzl and Fischer 2002), as well as hypocenter migration (Parotidis et al. 2003; Dahm et al. 2008).

Applying the ETAS-model to the year 2000 earthquake swarm, Hainzl and Ogata (2005) found a low α-value and a strong time-dependence of the background forcing. However, they chose rather arbitrarily a smoothing time window of 10 days and fixed the ETAS-triggering parameters for their analysis. We thus reanalyze the same swarm activity with the new methodology of Marsan et al.

(2012). In addition to the year 2000 swarm, we also investigated the latest large swarm, which occurred in 2008. In both cases, we analyzed the earthquake data provided by the WEBNET. The frequency-magnitude distribution of both swarms is shown in Fig. 4(a). The overall distributions can be approximately fitted by a b-value of about 1, but a closer inspection reveals a kink at $m \approx 1.5$. This magnitude seems to separate two different regimes: $b \approx 1.25$ for $m > 1.5$ and $b \approx 0.9$ for $m \leq 1.5$ with an estimated magnitude of completeness being around 0.5. The data set consists of 2450 events in the year 2000 and 2563 events in the year 2008 with $M_L \geq 0.5$. The temporal occurrence of the events is shown in Figure 4(b) and (c).

All results of our ETAS-model analysis are summarized in Table 3. The analysis of the activity with the standard ETAS-model (constant background rate) yields very low α-values, namely 0.55 and 0.28 for the year 2000 and 2008 swarms, respectively. As demonstrated in the last section, these estimations might be affected by partial incompleteness of the catalog and time-dependent aseismic forcing. Therefore we firstly restricted the likelihood space to magnitudes above 1.5, where the kink in the frequency magnitude distribution is observed. Additionally we excluded the potentially incomplete time periods directly after earthquakes, where we used again the empirical incompleteness function of Helmstetter et al. (2006) (see Sec. 3.2). As a result, the α-values significantly increase to values of 1.50 and 1.55. Besides potential incompleteness, we cannot exclude the possibility that this strong increase can also indicate some real differences in nucleation and interaction of the $m < 1.5$ swarm events, which might be indicated by their apparently different b-value.

Accounting additionally for time-dependent background forcing does not further increase the values, with $\alpha = 1.41$ and 1.56 then. Nevertheless, the inversion reveals a strong variation of the background forcing rate during both swarms (see lines in Fig. 4). While the inversion assuming constant background indicates only a negligible percentage of background events of 0.4% and 0.2%, a much higher percentage of 11% and 19% is associated to aseismic forcing when relaxing this a priori assumption.

4.2 California clusters

We used the catalog downloaded from the Southern California Earthquake Data Center (SCEDC) between 1980/1/1 and 2011/12/31 with 101,930 earthquakes with magnitude $m \geq 2$. The magnitude cutoff is used in accordance to the magnitude of completeness defined by the constraint that 95% of the events can be modeled by a power-law fit of the frequency-magnitude distribution, following the procedure of Wiemer and Wyss (2000). In this data set, we limit our search for mainshocks to the square area defined by $32.50° - 37.00°$ latitude and $113.58° - 121.76°$ longitude.

The separation into clusters is done in agreement with the method used by Enescu et al. (2009). An event is considered as indicator of a cluster if at least 100 events occurred within a temporal $\pm T$ and spatial $r \leq R$ window around it. Furthermore, this event has to be the largest event within the same spatiotemporal window to separate aftershock activity related to some preceding events. We consider only clusters, where the largest earthquake magnitude is between 3.5 and 6.0, because the use of circular spatial windows is considered only appropriate for the triggering zones of $m \leq 6$ events. We used a time window of $T = 100$ days and the search radius R is taken to be 5 times of the estimated fracture length L, where L is assumed to scale with the earthquake magnitude according to $L = 0.01 \cdot 10^{0.5m}$ km (Working Group on California Earthquake Probabilities, 2003; Helmstetter et al., 2005). Our selection criteria yields 36 clusters. For each of them we use, if available in the catalog, the seismicity of the 1000 days preceding the cluster in the same region as input information for the calculation of the ETAS rates. The so-called observation space is therefore: $[-1100 : 100]$ days and $m \geq 2$.

The parameter estimations might be affected by partial incompleteness of the catalog and time-dependent aseismic forcing as shown in our synthetic tests (see Sec. 3). To test this, we firstly analyzed the clusters assuming constant background forcing without any additional restrictions for the likelihood space. This unrestricted LL-space is defined as $[-100 : 100]$ days and $m \geq 2$. In a second step, we still assumed a constant background forcing, but restricted the likelihood space to $m \geq 2.5$ and excluded the potentially incomplete time periods after earthquakes according to the results from Helmstetter et al. (2006) described in Sec. 3.2. In the final step, we additionally allow for time-dependent background forcing in the parameter inversion. For all three cases, the

results for the inverted ETAS-parameters are summarized in Table 4. A systematic change of the parameters is observed. In particular, the α-value is found to increase from a median value of 1.65 to 1.96 in agreement with our observations in the synthetic tests. Thus the α-values converge to the values estimated for stacked aftershock activity, for which e.g. Helmstetter et al. (2005) found $\alpha_{10} = 1.05 \pm 0.05$ related to the basis of 10, which is equivalent to $\alpha = 2.4 \pm 0.1$. Although the stacking procedure relates all aftershocks to the mainshock and measures therefore the dressed activity in contrast to the ETAS parameters, which are related to the direct (undressed) aftershock activity, the results of both approaches are expected to be in the same range. Furthermore, an α-value around 2.3 would be also in agreement with results for static stress triggering models (Hainzl et al. 2010). Because of this, we now ask the question the other way around: How many of the clusters are in agreement with a value of $\alpha = 2.3$, that means, a 10^m-scaling? To answer this question, we repeated our analysis for restricted LL-space and allowed time-dependent background forcing with fixed $\alpha = 2.3$. Clearly this always leads to a worse fit with a smaller LL-value, because the fitting has one free parameter less. For the judgment of the significance of allowing α to deviate from 2.3, we use again the Akaike information criterion. We find that 21 out of the 36 clusters can be best described by $\alpha = 2.3$. Thus the majority of clusters can be described by a 10^m-scaling of the productivity. In the other cases, we further identified the clusters, where the difference in the AIC-value is at least 2, i.e. $\Delta AIC = AIC_{\alpha=2.3} - AIC \geq 2$. Note that $\exp(-\Delta AIC/2)$ can be interpreted as the relative probability that the $\alpha = 2.3$ model minimizes the (estimated) information loss (Burnham and Anderson 2002). Nine clusters are found with $\Delta AIC \geq 2$; two of them with $\alpha > 2.3$ and 7 with $\alpha < 2.3$. These deviations from 2.3 seem to be not random. In particular, we find that the clusters with significant low α-values correlate well with areas of high heat flow. This is shown in Figure 5, where the estimated α-values are plotted as a function of the heat flow measurement closest to the mainshock. This trend compares well with observations of low α-values ($\alpha \approx 1.6$) on oceanic transform faults (McGuire et al. 2005), for which high heat flow is expected (Behn et al. 2007). Our results verify the results of Enescu et al. (2009) who found already correlations between high heat flow and low α-values. However, the past study did

neither consider partial incompleteness nor account for potential aseismic forcing. Our new results indicate that the previous results were no artefacts related to those factors.

5 DISCUSSION

Our analysis shows that the maximum likelihood estimation of the ETAS-parameters can be strongly affected by catalog problems and aseismic transients. While possible catalog problems can be considered by appropriate restrictions of the LL-space in the standard ETAS-model applications, the latter issue needs more sophisticated approaches such as the iterative ETAS-based algorithm by Marsan et al. (2012) used in this paper.

In addition to the two discussed issues, a number of other problems have been previously shown to have also influence on the results of earthquake clustering models. In our study, we ignored the spatial information of the earthquake catalogs in order to avoid some of these problems, in particular the bias resultant from anisotropic aftershock clustering (Hainzl et al. 2008) or space-dependent background seismicity (Harte 2012). Nevertheless, other problems cannot be avoided such as missing links in magnitude, space and time. Notably the missed triggering effect from events smaller than the cut-off magnitude is important (Sornette and Werner 2005). Unobserved events can trigger events above the threshold giving rise to apparently independent background events that seem to increase the constant background rate to an apparent rate. Although this can strongly affect the estimation of the background level, the bias for the trigger parameters $K, c, \alpha,$ and p does not exceed a few percent (Wang et al. 2010), which is much smaller than the bias observed in our analysis. Finally, Touati et al. (2011) showed that a high background rate can mask the earthquake triggering behavior. However, this seems to have only minor effects in our case because our approach has been demonstrated to yield robust estimations for synthetic simulations (see section 3). In comparison, catalog problems and aseismic transients, as discussed in this paper, seem to have a stronger impact on the estimation of the trigger parameters and should therefore not be ignored in future studies.

6 CONCLUSION

While earthquake interactions are known to be responsible for a large fraction of recorded seismicity, the corresponding seismicity parameters describing the aftershock productivity are not well-constrained and a matter of ongoing debate. In particular, the α-parameter determining the magnitude-dependence of the trigger potential is crucial for identifying the underlying triggering mechanism and for forecasting ongoing earthquake sequences. Previous analysis of stacked seismicity resulted in significantly higher values than ETAS-based inversions. Our analysis now demonstrates that α can be strongly underestimated by the ETAS model, if potential catalog problems and aseismic transients are ignored. This might especially explain the previously observed small α-values in the case of earthquake swarms and water-injection induced seismicity, where transient forcing is expected or known (Ogata 1992; Hainzl and Ogata 2005; Lei et al. 2008).

Our applications to earthquake swarms in Western Bohemia and earthquake clusters in California indicate a significant increase of the α-parameter after accounting for potential incompleteness and transient aseismic forcing. The majority of earthquake clusters in California become compatible with $\alpha = \beta = \ln(10)b \approx 2.3$. Thus both estimation procedures, the ETAS and the stacking approach, lead to concordant results. This is not trivial because one method estimates the parameter on basis of secondary aftershock triggering within an individual sequence, while the other method compares the cumulative productivity of different mainshocks. Furthermore, $\alpha = \beta$ implies that the impact of lower magnitude events is not as strong as previously thought. And finally, $\alpha \approx 2.3$ would be in agreement with estimations for static stress triggering (Hainzl et al. 2010).

However, some of the analyzed seismicity clusters show significantly smaller α-values also after accounting for incompleteness and transient aseismic forcing. Both analyzed earthquake swarms in Western Bohemia have similar values of $\alpha = 1.4 - 1.5$ and seven clusters in California show significant deviations to smaller α-values. These clusters show clear correlations with regions of higher heat flow. Thus proper accounting for incompleteness and transient aseismic forcing can help to avoid artificial parameter estimations as well as to detect true variations of the earthquake interaction mechanism.

7 DATA AND RESOURCES

The heat flow data are taken from the USGS online heat flow database: http://earthquake.usgs.gov/research/bor
(accessed at February 2012). The California earthquake catalog has been downloaded from the
Southern California Earthquake Data Center (SCEDC, http://www.data.scec.org/eq-catalogs/date_mag_loc.php
The WEBNET swarm catalogs have been provided by Tomas Fischer.

ACKNOWLEDGMENTS

We wish to thank ... The work was partially supported by the EU-project REAKT and the German research project PROGRESS. The second author was supported by the graduate school GeoSim.

REFERENCES

Behn, M., M. S. Boettcher, and G. Hirth (2007). Thermal structure of oceanic transform faults, *Geology* **35** 307–310.

Braeuer, K.. H. Kampf, U. Koch, S. Niedermann, G. Strauch (2007). Seismically induced changes of the fluid signature detected by a multi-isotope approach (He, CO2, CH4, N-2) at the Wettinquelle, Bad Brambach (central Europe), *J. Geophys. Res.* **112** B04307, doi: 10.1029/2006JB004404.

Burnham, K. P., and D. R. Anderson (2002). *Model selection and multimodel inference: a practical information-theoretic approach*, Springer-Verlag New York, Berlin, Heidelberg, paragraph 6.4.5, 2002.

Christophersen, A., and E.G.C. Smith (2008). Foreshock rates from aftershock abundance with different search algorithms, *Bull. Seismol. Soc. Am.* **98** 2133–2148, doi: 10.1785/0120060143.

Dahm, T., T. Fischer, and S. Hainzl (2008). Mechanical intrusion models and their implications for the possibility of magma-driven swarms in NW Bohemia region, *Stud. Geophys. Geod.* **52** 529–548.

Daniel, G., D. Marsan, and M. Bouchon (2008). Earthquake triggering in southern Iceland following the June 2000 Ms 6.6 doublet, *J. Geophys. Res.* **113** B05310, doi:10.1029/2007JB005107

Dieterich, J. H. (1994). A constitutive law for rate of earthquake production and its application to earthquake clustering, *J. Geophys. Res.* **99** 2601–2618.

Hainzl, S., and Y. Ogata (2005). Detecting fluid signals in seismicity data through statistical earthquake modeling, *J. Geophys. Res.* **110** B05S07, doi: 10.1029/2004JB003247.

Hainzl, S., and T. Fischer (2002). Indications for a successively triggered rupture growth underlying the 2000 earthquake swarm in Vogtland/NW Bohemia, *J. Geophys. Res.* **107** 2338, doi:1029/2002JB001865.

Hainzl, S., A. Christophersen, and B. Enescu (2008). Impact of earthquake rupture extensions on parameter estimations of point-process models, *Bull. Seismol. Soc. Am.* **98** 2066–2072.

Hainzl, S., G. B. Brietzke, and G. Zoeller (2010). Quantitative earthquake forecasts resulting from static stress-triggering *J. Geophys. Res.* **115** B11311, doi: 10.1029/2010JB007473.

Harris, R.A. (1998). Introduction to special section: Stress triggers, stress shadows, and implications for seismic hazard, *J. Geophys. Res.* **103** 24347–24358.

Harte, D. (2012). Bias in fitting the ETAS model: a case Study based on New Zealand seismicity, *Geophys. J. Int.* submitted.

Helmstetter, A., Y. Y. Kagan, and D. D. Jackson (2005). Importance of small earthquakes for stress transfers and earthquake triggering, *J. Geophys. Res.* **110** B05S08, doi:1029/2004JB003286.

Helmstetter, A., Y. Y. Kagan, and D. D. Jackson (2006). Comparison of short-term and time-independent earthquake forecast models for southern California, *Bull. Seismol. Soc. Am.* **96** 90–106.

Holtkamp S. G., and M. R. Brudzinski (2011). Earthquake swarms in circum-Pacific subduction zones, *Earth Plan Science Lett.* **305** 215–225.

Marsan, D., O. Lengliné (2008). Extending earthquakes' reach through cascading, *Science* **319** 1076–1079.

Kagan, Y.Y. (2004). Short-term properties of earthquake catalogs and models of earthquake source, *Bull. Seismol. Soc. Am.* **94** 1207–1228.

Lei, X., G. Yu, S. Ma, X. Wen, and Q. Wang (2008). Earthquakes induced by water injection at 3 km depth within the Rongchang gas field, Chongqing, China, *J. Geophys. Res.* **113** B10310, doi: 10.1029/2008JB005604.

McGuire, J. J., M. S. Boettcher, and T. H. Jordan (2005). Foreshock sequences and short-term earthquake predictability on East Pacific Rise transform faults *Nature* **434** 457–461, doi:10.1038/nature03377.

Miller, S. A., C. Collettini, L. Chiaraluce, M. Cocco, M. Barchi, and B. J. P. Kaus (2004). Aftershocks driven by a high-pressure CO2 source at depth, *Nature* **427** 724–727.

Lombardi, A. M., W. Marzocchi, and J. Selva (2006). Exploring the evolution of a volcanic seismic swarm: The case of the 2000 Izu Islands swarm, *Geophys. Res. Lett.* **33** L07310, doi: 10.1029/2005GL025157.

Ogata, Y. (1988). Statistical models of point occurrences and residual analysis for point processes, *J. Am. Stat. Assoc.* **83** 9–27.

Ogata, Y. (1992). Detection of precursory relative quiescence before great earthquakes through a statistical model, *J. Geophys. Res.* **97** 19845–19871.

Ogata, Y. and K. Katsura (1993). Analysis of temporal and spatial heterogeneity of magnitude frequency distribution inferred from earthquake catalogues, *Geophys. J. Int.* **113** 727–738.

Parotidis, M., E. Rothert, and S. A. Shapiro (2003). Pore-pressure diffusion: A possible triggering mechanism for the earthquake swarms 2000 in Vogtland/NW-Bohemia, central Europe. *Geophys. Res. Lett.* **30** 2075, doi:10.1029/2003GL018110.

Marsan, D., E. Prono, and A. Helmstetter (2012). Methods for monitoring aseismic forcing in fault zones based on earthquake time series, *Bull. Seismol. Soc. Am.*, submitted.

Reasenberg, P. (1985). Second-order moment of central California seismicity, 1969-1982, *J. Geophys. Res.* **90** 5,479–5,495.

Sornette, D., and M. J. Werner (2005). Apparent clustering and apparent background earthquakes biased by undetected seismicity, *J. Geophys. Res.* **110** B09303, doi: 10.1029/2005JB003621.

Stein, R. S. (1999). The role of stress transfer in earthquake occurrence, *Nature* **402** 605–609.

Toda, S., R. S. Stein, and T. Sagiya (2002). Evidence from the AD 2000 Izu islands earthquake swarm that stressing rate governs seismicity, *Nature* **419** 6902, 58–61.

Touati, S., M. Naylor, I. G. Main, and M. Christie (2011). Masking of earthquake triggering behavior by a high background rate and implications for epidemic-type aftershock sequence inversions *J. Geophys. Res.* **116** B03304, doi: 10.1029/2010JB007544.

Utsu, T., Y. Ogata, and R. S. Matsu'ura (1995). The centenary of the Omori formula for a decay of aftershock activity, *J. Phys. Earth* **43** 1–33.

Wang, Q., D. D. Jackson, and J. Zhuang (2010). Missing links in earthquake clustering models, *Geophys. Res. Lett.* **37** L21,307.

Wiemer, S., and M. Wyss (2000). Minimum magnitude of complete reporting in earthquake catalogs: Examples from Alaska, the western United States, and Japan, *Bull. Seismol. Soc. Am.* **90** 859-869.

Working Group on California Earthquake Probabilities (2003). Earthquake probabilities in the San Francisco Bay region: 20022031, *U.S. Geol. Surv. Open-File Rept.*, 3–214.

Authors' affiliations, addresses

Sebastian Hainzl:

GFZ German Research Centre for Geosciences

Telegrafenberg

14473 Potsdam

Germany

Email: hainzl@gfz-potsdam.de

Olga Zakharova:

GFZ German Research Centre for Geosciences

Telegrafenberg

14473 Potsdam

Germany

Email: olgaza@gfz-potsdam.de

David Marsan:

Laboratoire de Géophysique Interne et Tectonophysique

UMR CNRS 5559

Université de Savoie

73376 Le Bourget du Lac

France

Email: david.marsan@univ-savoie.fr

Table 1. Characteristics and parameters of the ETAS-simulations, where H denotes the Heaviside function. The choice of M_m for ETAS-2 is such that a mainshock of magnitude M_m occurring at $t = 50$ days would on average trigger N_b direct aftershocks in the following 50 days (remaining duration of the catalog).

time-intervals	catalog	$[-100 : 100]$ days
	LL-optimization	$T = [0 : 100]$ days
magnitudes		$0 \leq m \leq 4$; Gutenberg-Richter distributed with $b = 1$
ETAS-parameter	triggering	$K = 0.015, \alpha = 1.84, c = 0.01$ day$^{-1}, p = 1.2$
background	number	$N_b = 100$ or 500 in T
	ETAS-0	$\mu(t) = N_b/T$
	ETAS-1	$\mu(t) = (N_b/T)(0.3 + (0.7/50)(1.0 - \cos(2\pi(t/50 - 0.5)))H(t - 25)H(75 - t)$
	ETAS-2	$\mu(t) = (N_b/T)(0.3 + 0.7K \exp(-\alpha M_m)(c + t - 50)^{-p}H(t - 50)$
		with $M_m = ln\left(N_b(p-1)/(K(c^{p-1} - (c+50)^{p-1}))\right)/\alpha$

Table 2. Estimated ETAS-parameters for synthetic catalogs with artificially removed events representing typical catalog problems. The true parameters are that given in Tab.1, only in the last two cases of (iii), the c and K-value are changed to increase the effect of incompleteness.

	type of missing events	K [$K_{10\%}$ $K_{90\%}$]	α [$\alpha_{10\%}$ $\alpha_{90\%}$]	c [$c_{10\%}$ $c_{90\%}$] [days]	p [$p_{10\%}$ $p_{90\%}$]
(i)	time-independent incompleteness	0.008 [0.005 0.011]	1.84 [1.71 1.97]	0.012 [0.006 0.018]	1.20 [1.05 1.32]
(ii)	incomplete time period	0.030 [0.015 0.047]	1.45 [1.05 1.80]	0.010 [0.006 0.016]	1.15 [1.02 1.33]
	...with LL-space restriction	0.011 [0.007 0.016]	1.91 [1.73 2.10]	0.017 [0.005 0.039]	1.32 [1.03 1.56]
(iii)	incomplete first aftershocks	0.018 [0.012 0.026]	1.71 [1.53 1.88]	0.017 [0.008 0.025]	1.28 [1.13 1.41]
	...for $c = 0.0007$ day; $K = 0.008$	0.014 [0.009 0.021]	1.54 [1.35 1.71]	0.0011 [0.0007 0.0015]	1.20 [1.12 1.27]
	...with LL-space restriction	0.008 [0.006 0.010]	1.87 [1.74 1.98]	0.0008 [0.0005 0.0010]	1.21 [1.14 1.27]

Table 3. Results for the estimated ETAS parameters in the case of the earthquake swarms in Western Bohemia. To avoid incompleteness problems, the likelihood value has been optimized in the second and third case for each swarm only for the $m \geq 1.5$ earthquakes. The $0.5 \leq m < 1.5$ events were only used for the calculation of the rate function.

year	background	background fraction	K	α	c	p
2000	constant	0.4%	0.0185	0.55	0.00048	1.35
	...with LL-space restriction	2%	0.0050	1.50	0.00026	1.33
	$\mu(t)$	11%	0.0036	1.41	0.00026	1.37
2008	constant	0.2%	0.0269	0.28	0.00041	1.29
	...with LL-space restriction	0.6%	0.0065	1.55	0.00081	1.37
	$\mu(t)$	19%	0.0045	1.56	0.00045	1.36

Table 4. Median values as well as the 10% and 90% quantiles of the estimated ETAS parameters for the 36 earthquake clusters in California. The first two cases refer to the inversion based on constant background forcing without (a) and with (b) additional restrictions of the likelihood space. The case (c) shows the results in the case that time-dependent background forcing is allowed with restricted likelihood space.

		K [$K_{10\%}$ $K_{90\%}$]	α [$\alpha_{10\%}$ $\alpha_{90\%}$]	c [$c_{10\%}$ $c_{90\%}$] [days]	p [$p_{10\%}$ $p_{90\%}$]
(a)	constant background	0.023 [0.000029 0.040]	1.65 [0.91 2.87]	0.0057 [0.00023 0.033]	1.06 [0.85 1.27]
(b)	...with LL-space restriction	0.011 [0.000004 0.027]	1.75 [1.00 3.41]	0.0033 [0.00011 0.030]	1.11 [0.88 1.29]
(c)	$\mu(t)$	0.005 [0.000001 0.024]	1.96 [0.84 3.40]	0.0028 [0.00001 0.032]	1.20 [0.99 1.54]

Figure 1. Examples of tested ETAS simulations: (a) transient triggering with smooth transient forcing (ETAS-1) and (b) with mainshock-type aseismic forcing (ETAS-2). Both simulations consists of 100 background events. The dotted lines refer to the true background forcing rates.

Figure 2. Inversion results for ETAS-simulations with constant forcing (ETAS-0, left in each plot) and transient forcing (middle: ETAS-1 and right: ETAS-2). Black symbols indicate the inversion results assuming constant background rate, while red symbols refer to results if potential time-dependent forcing is considered. We only show here the results with $N_b = 500$ background events; simulations with 100 background earthquakes yield similar results, albeit with larger error bars. The true parameters of the simulations are indicated by the horizontal line. In all cases, crosses refer to the median value of 100 simulations while the error bars show the range between the 10% and 90% quantiles.

Figure 3. Examples of earthquake catalogs artificially corrupted to represent realistic catalog problems. Red points refer to events deleted from the analyzed catalogs. The plots (a) to (c) refer to case (i) to (iii) in the text and Tab. 2, respectively.

Figure 4. Western Bohemia swarm activity observed in the year 2000 and 2008: (a) the frequency-magnitude distributions (b-values of 0.88 and 1.25 indicated by dashed lines); (b) and (c) magnitude versus time plots, where the dotted lines refer to the inverted background rates. Note that the cutoff magnitude for the analysis is set to 0.5.

Figure 5. Scatter plot of estimated α-values and the spatially closest heat-flow value. Black symbols indicate clusters which can be explained by $\alpha = 2.3$, i.e. $\Delta AIC = AIC_{2.3} - AIC \leq 0$, while the colored points indicate clusters, where the Akaike information criteria points to a different α-value: $\alpha < 2.3$ (red) and $\alpha > 2.3$ (green). Large symbols refer to those clusters with higher significance, $\Delta AIC \geq 2$.

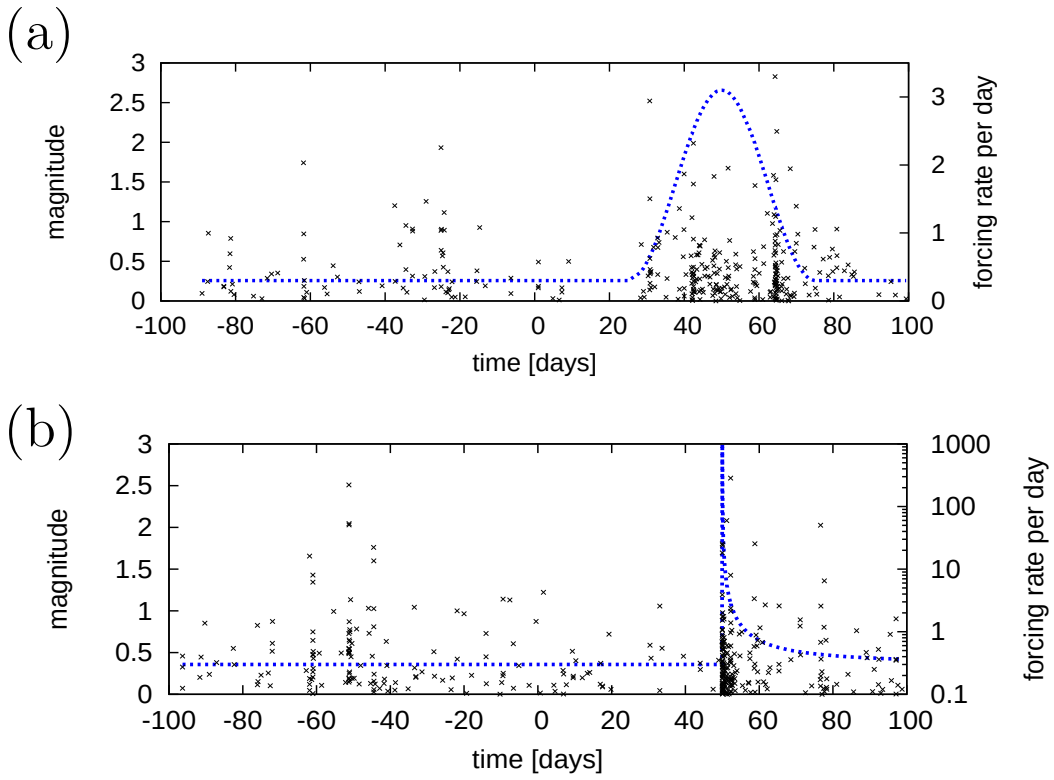
(a)
magnitude
forcing rate per day
time [days]
(b)
magnitude
forcing rate per day
time [days]

Figure 1.

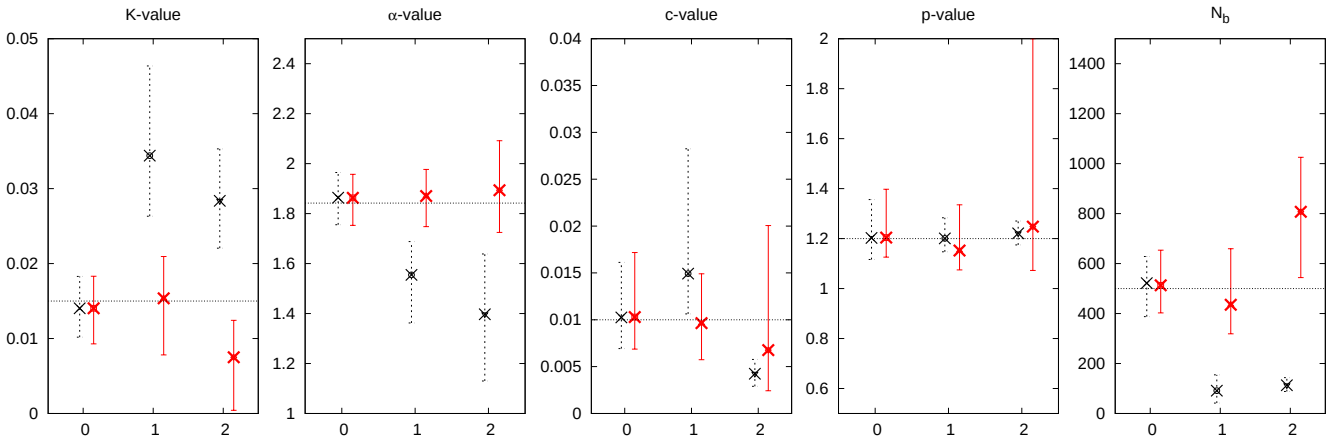
K-value
α-value
c-value
p-value
N_b
0.05
0.04
0.03
0.02
0.01
0
2.4
2.2
2
1.8
1.6
1.4
1.2
1
0.04
0.035
0.03
0.025
0.02
0.015
0.01
0.005
0
2
1.8
1.6
1.4
1.2
1
0.8
0.6
1400
1200
1000
800
600
400
200
0
0
1
2

Figure 2.

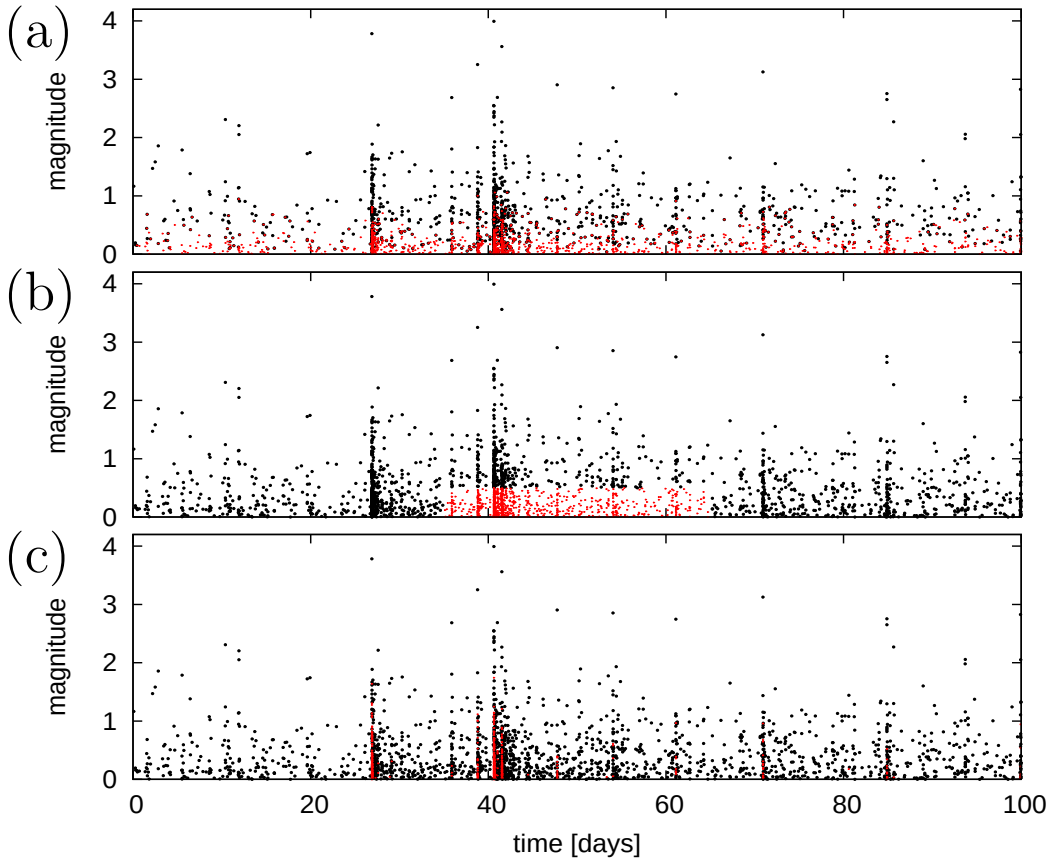
(a)
(b)
(c)
magnitude
magnitude
magnitude
0
1
2
3
4
0
20
40
60
80
100
time [days]

Figure 3.

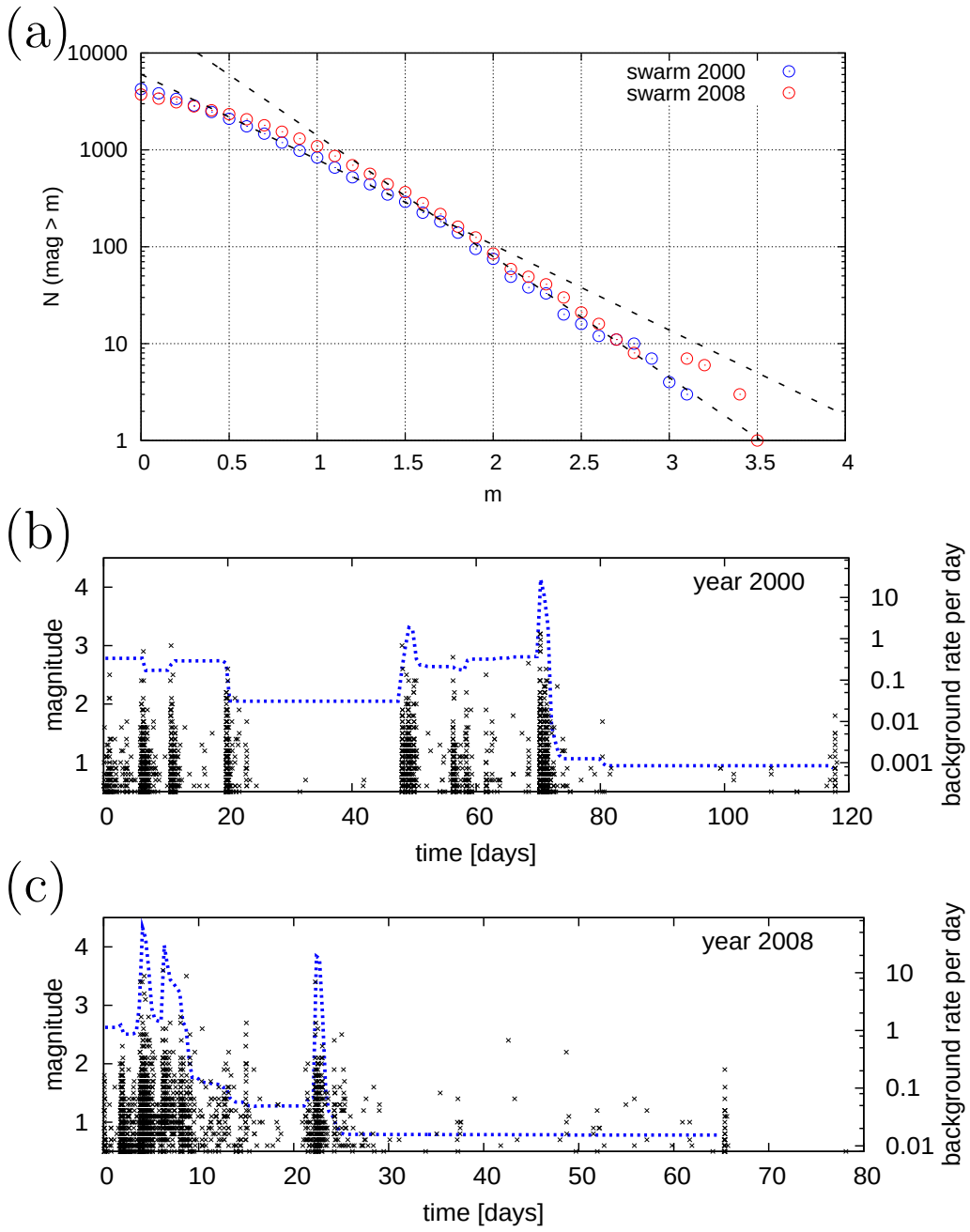
(a)
swarm 2000
swarm 2008
N (mag > m)
m
(b)
year 2000
magnitude
background rate per day
time [days]
(c)
year 2008
magnitude
background rate per day
time [days]

Figure 4.

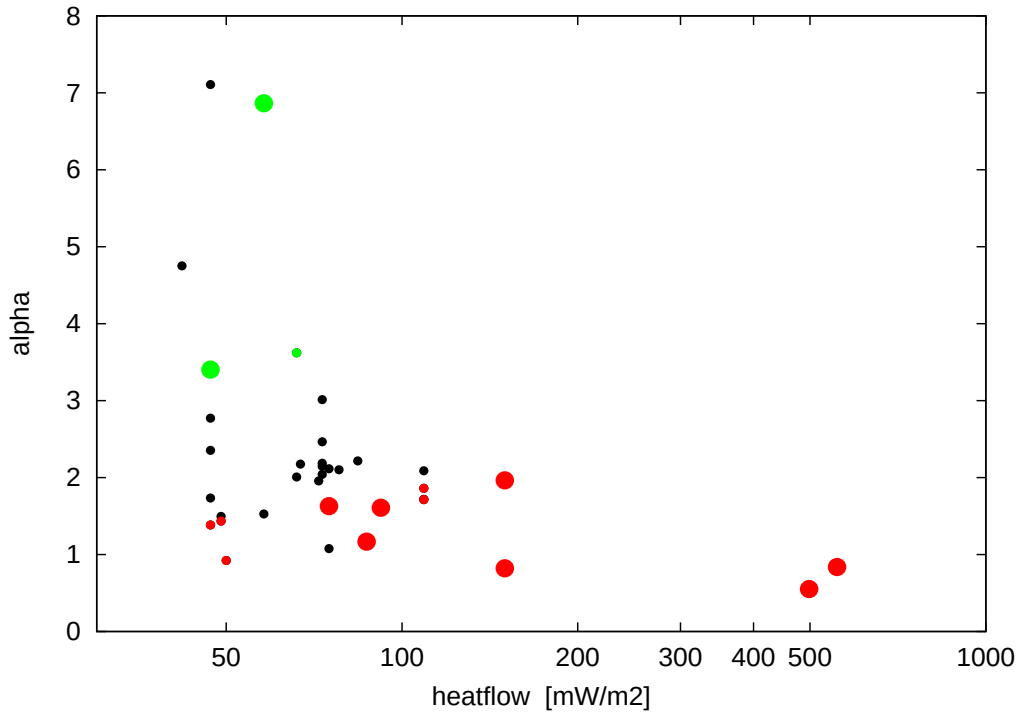

Figure 5.